


Article

The Synthesis and Photophysical Properties of Weakly Coupled Diketopyrrolopyrroles

Michał Pieczykolan ¹, James B. Derr ² , Amara Chrayteh ³, Beata Koszarna ¹, John A. Clark ⁴ , Olena Vakuliuk ¹, Denis Jacquemin ^{3,*}, Valentine I. Vullev ^{2,4,*}  and Daniel T. Gryko ^{1,*} 

¹ Institute of Organic Chemistry, Polish Academy of Sciences, Kasprzaka 44-52, 01-224 Warsaw, Poland; Michal.Pieczkolan@rwth-aachen.de (M.P.); beata.koszarna@icho.edu.pl (B.K.); olena.vakuliuk@icho.edu.pl (O.V.)

² Department of Biochemistry, University of California, Riverside, CA 92521, USA; jderr002@ucr.edu

³ CEISAM Laboratory—UMR 6230, University of Nantes, CNTS, 44035 Nantes, France; amara.chrayteh@univ-nantes.fr

⁴ Department of Bioengineering, University of California, Riverside, CA 92521, USA; jclar019@ucr.edu

* Correspondence: Denis.Jacquemin@univ-nantes.fr (D.J.); vullev@ucr.edu (V.I.V.); dtgryko@icho.edu.pl (D.T.G.)

Abstract: Three centrosymmetric diketopyrrolopyrroles possessing either two 2-(2'-methoxyphenyl) benzothiazole or two 2-(2'-methoxyphenyl)benzoxazolo-thiophene scaffolds were synthesized in a straightforward manner, and their photophysical properties were investigated. Their emission was significantly bathochromically shifted as compared with that of simple DPPs reaching 650 nm. Judging from theoretical calculations performed with time-dependent density functional theory, in all three cases the excited state was localized on the DPP core and there was no significant CT character. Consequently, emission was almost independent of solvents' polarity. DPPs possessing 2,5-thiophene units vicinal to DPP core play a role in electronic transitions, resulting in bathochromically shifted absorption and emission. Interestingly, as judged from transient absorption dynamics, intersystem crossing was responsible for the deactivation of the excited states of DPPs possessing *para* linkers but not in the case of dye bearing *meta* linker.

Keywords: dyes; fluorescence; direct arylation; diketopyrrolopyrroles



Citation: Pieczykolan, M.; Derr, J.B.; Chrayteh, A.; Koszarna, B.; Clark, J.A.; Vakuliuk, O.; Jacquemin, D.; Vullev, V.I.; Gryko, D.T. The Synthesis and Photophysical Properties of Weakly Coupled Diketopyrrolopyrroles. *Molecules* **2021**, *26*, 4744. <https://doi.org/10.3390/molecules26164744>

Academic Editor: Yuri Fedorov

Received: 9 July 2021

Accepted: 25 July 2021

Published: 5 August 2021

Publisher's Note: MDPI stays neutral with regard to jurisdictional claims in published maps and institutional affiliations.



Copyright: © 2021 by the authors. Licensee MDPI, Basel, Switzerland. This article is an open access article distributed under the terms and conditions of the Creative Commons Attribution (CC BY) license (<https://creativecommons.org/licenses/by/4.0/>).

1. Introduction

In the chemistry of dyes and pigments, systems with extended π -conjugation have prevailed in the literature for years [1–8]. There is, however, an increased interest in weakly coupled systems containing multiple biaryl linkages [9–14]. Depending on the dihedral angle both in the ground and in the excited states, the magnitude of electronic communication varies, leading to large Stokes' shifts and strong solvatochromism of fluorescence. In particular, modulations of the planarization and polarization of such chromophores with push–pull configurations has become a conceptually new approach towards modern fluorescent probes. They exhibit sensitivity not only to solvent polarity but also to medium viscosity. Matile and co-workers have shown that such probes respond to changes in the fluidity of lipid bilayer membranes [15–20].

Looking for chromophores, which possess the suitable architecture for probing via weakening of their intramolecular electronic coupling, we focused on diketopyrrolopyrrole (DPP) derivatives (Figure 1) [21–29]. These donor–acceptor cross-conjugated dyes with DPP cores are characterized by straightforward synthesis [30–37], almost a unity emission quantum yield [21], large two-photon absorption cross-section [38–45], and broad utility in organic optoelectronics [46–71]. Depending on the dihedral angle between C-aryl substituents and the core, the absorption of DPPs ranges from 500 to 600 nm [21]. The relationship between the structure of the DPPs and their linear and non-linear optical

properties has been probed in numerous studies [72–78]. Replacing the phenyls with aromatic five-membered rings at positions 3 and 6 in *N,N'*-dialkylated DPPs decreased the dihedral angle from ca. 30 to ~7 degrees, thus altering the photophysical properties [21]. In particular, a bathochromic shift of absorption is often observed [79–82], accompanied by better packing in the crystalline state, stronger charge transfer, and larger two-photon absorption cross-sections [38–45]. It is, therefore, interesting to study multiple architecture based on the DPP scaffold—possessing groups such as benzoxazole and benzothiazole either directly linked via benzene ring or elongated via thiophene rings.

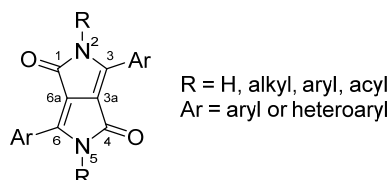
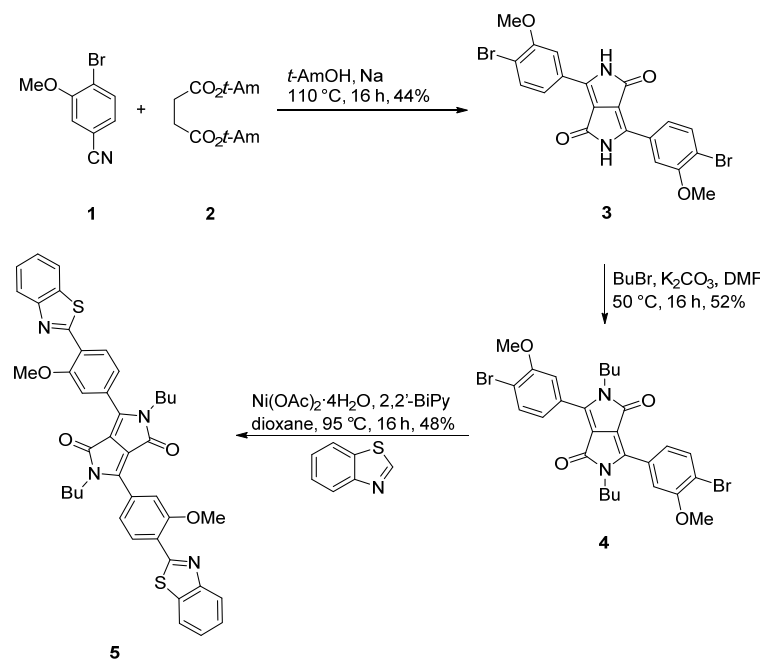


Figure 1. General structure of diketopyrrolopyrroles with atom numeration.

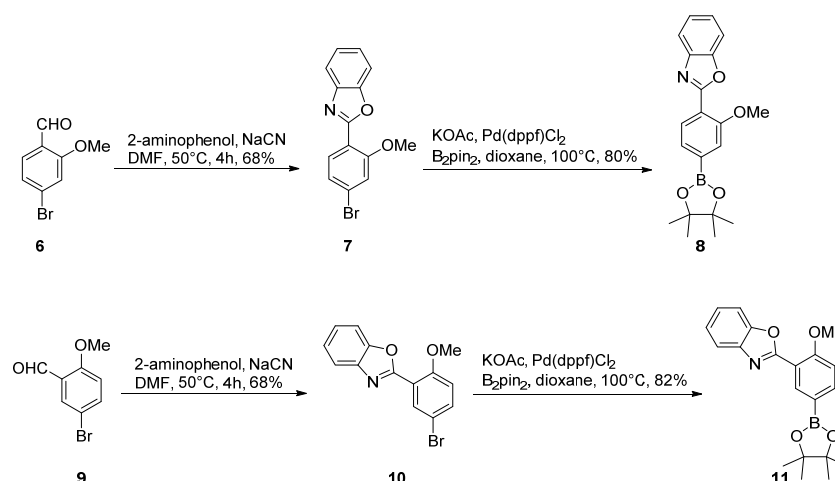
2. Results

2.1. Design and Synthesis

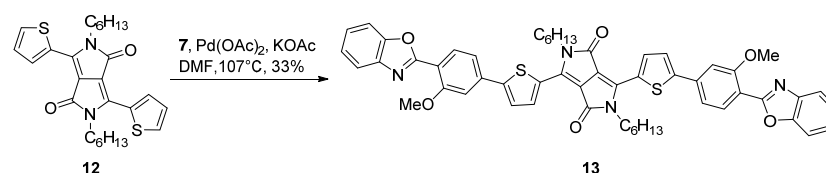
Our design of *N,N'*-dialkyldiketopyrrolopyrroles was based on placing two different rings between benzoxazole/benzothiazole units and DPP core. In the first case, we bridged them with 1,4-phenylene linkers (**5**, Scheme 1). An addition of 2,5-thiophen units between the DPP core and the benzene rings (**13** and **15**, Schemes 2–4), while extending the linkers, enhanced the electronic communication by decreasing the dihedral angles. The benzoxazole unit and methoxy unit were alternately placed at positions 1,4 and 1,3.



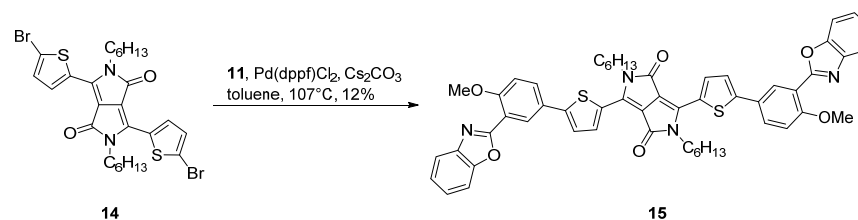
Scheme 1. The synthesis of diketopyrrolopyrrole **5**.



Scheme 2. The synthesis of benzoxazoles **8** and **11**.



Scheme 3. The synthesis of DPP **13**.



Scheme 4. The synthesis of DPP **15**.

Therefore, we initiated our investigation with the preparation of DPP **3**, which contains two 3-methoxyphenyl substituents. We recently learned that if classical diisopropyl succinate is used in reactions with 3,4-dimethoxybenzoxazole, the replacement of one or more methoxy groups with isopropyl groups is a side reaction. Therefore, we resolved this by using more sterically hindered bis(*tert*-amyl)succinate (**2**) in reaction with nitrile **1** (Scheme 1). The pigment **3** was subsequently *N*-alkylated under classical conditions to give DPP **4** in 23% overall yield (Figure S1). DPP **4** was subsequently used as arylating agent in direct arylation of benzothiazole under recently described conditions [83], leading to the formation of DPP **5** (Scheme 1, Figure S2).

Independently, two regioisomeric methoxybenzaldehydes **6** and **9** possessing bromine atom were condensed with 2-aminophenol to give corresponding benzoxazoles **7** and **10** (Scheme 2, Figures S3 and S5). Subsequently bromine atoms were replaced with pinacolborane to give highly functionalized heterocyclic building blocks **8** and **11** (Figures S4 and S6).

Interestingly, the synthesis of DPP **13** from DPP **14** and **8** via Suzuki coupling led to the formation of dye **13** in 1% yield only. Therefore, we resorted to direct arylation, which had recently become a major tool in the synthesis of dyes [84,85] (including DPPs) [86–88], and heterocyclic PAHs [89]. Gratifyingly, DPP **12** underwent smooth reaction with compound **7** under the reaction conditions developed by Doucet and co-workers [90], to afford the desired DPP **13** in 33% yield (Scheme 3, Figure S7). In contrast to that result, the Suzuki coupling of DPP **14** with benzoxazole **11** gave DPP **15** in reasonable yield (Scheme 4, Figure S8).

2.2. Photophysical Properties

For the photophysical studies of diketopyrrolopyrroles **5**, **13**, and **15** using steady-state and time-resolved optical spectroscopy, we employed toluene (TOL) (Figure S9), dichloromethane (DCM), and *N,N*-dimethylformamide (DMF) (Figure S10) as solvents (Table 1, Figure 2). The red solutions of **5** showed fluorescence quantum yields (Φ_f) ranging between 0.7 and 0.9 and excited-state lifetimes (τ) around 4 ns, which is on par with what is expected for DPP chromophores (Table 1). The Stokes' shifts of about 2000 cm^{-1} suggest that the chromophore was exhibiting some changes in the geometry between the Franck–Condon and the fluorescent excited state. The lack of polarity dependence of τ and of the spectral maxima, λ_{abs} and λ_{fl} , precluded transitions involving excited states with a pronounced charge-transfer (CT) character. The 20% decrease in Φ_f of **5** upon transitioning to the polar DMF medium, while noticeable, cannot be ascribed to intramolecular excited-state CT. Dyes **5**, **13**, and **15** showed propensity for aggregation in solvents different from DCM. They all formed clear solution, but broad weak absorption bands in the near-infrared (NIR) region indicate ground-state aggregation. For **13** and **15**, the ground-state aggregation was noticeable for toluene and especially apparent for DMF. While the lifetimes extracted from the emission decays accounted only for the state responsible for the fluorescence around 600–700 nm, the absorption was cumulative for all species, resulting in the slightly decreased values of Φ_f for DMF.

Table 1. Photophysical properties of DPPs **5**, **13**, and **15**.

DPP	Solvent	λ_{abs} (nm)	λ_{em} (nm)	Φ_f	τ (ns)	$k_f \times 10^7/\text{s}^{-1}$	$k_{nr} \times 10^7/\text{s}^{-1}$
5	TOL	528	593	0.89	4.16	21.1	2.95
	DCM	515	589	0.86	4.35	19.7	3.27
	DMF	512	591	0.72	4.39	16.0	6.09
13	TOL	622	655	0.31	2.87	10.8	24.1
	DCM	614	648	0.24	2.94	8.23	25.8
	DMF	619	645	0.25	2.71	9.83	27.6
15	TOL	611	635	0.34	3.35	10.1	19.7
	DCM	606	633	0.32	3.23	9.92	21.0
	DMF	610	633	0.19	3.10	6.26	26.0

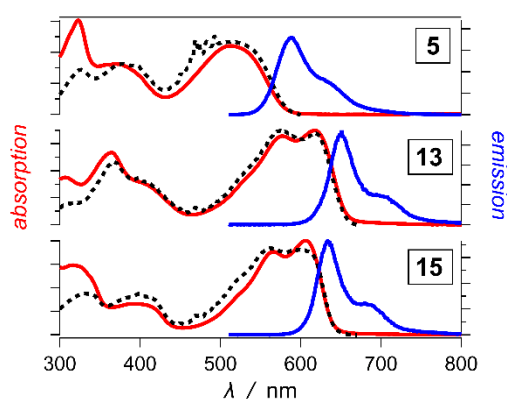


Figure 2. Absorption (red), excitation (dotted black), and emission (blue) spectra of compounds **5**, **13**, and **15** for DCM.

Introducing thiophene linker between the DPP core and 2-(2'-methoxyphenyl) moieties resulted in bathochromic shifts of the first absorption maximum from about 510–530 nm for **5** to 610–620 nm for **13** and **15** (Table 1, Figure 2). These shifts were more pronounced for the *para*-benzoxazole derivative, **13**, than for the *meta*-one, **15**. This feature is consistent with improving the electronic coupling across a phenylene linker upon shifting the substituents from *meta* to *para* position. The fluorescence maxima showed the same trends of

bathochromic shifts upon extending the linker and moving the benzoxazole units from the *meta* to the *para* sites (Table 1, Figure 2).

In the case of DPPs **13** and **15**, a vibronic structure of the absorption band emerged, and their Stokes' shifts decreased to 800 cm^{-1} . The fluorescence quantum yields of **13** and **15** decreased by about a factor of three in comparison with Φ_{fl} of **5**; and the excited-state lifetimes of **13** and **15** decreased by about 25% (Table 1). They indicate a 2-fold decrease in the radiative decay rate constants, k_f , of **13** and **15** that accompanied a 7-fold increase in the non-radiative decay rate constants, k_{nr} (Table 1).

Extending the π -conjugation and switching from benzothiazole of **5** to the more electron-withdrawing benzoxazole of **13** and **15** can decrease the overlaps between the natural transition orbitals (NTOs) for the $S_1 \rightarrow S_0$ radiate transitions responsible for the decrease in k_f . At the same time, the extra dihedral degrees of freedom in the aromatic linkers of **13** and **15** offer additional configurations that can bring the potential-energy surfaces (PESs) of the S_1 and S_0 states close to each other, providing internal conversion (IC) pathways for efficient non-radiative deactivation, as the increase in k_{nr} reflects (Table 1).

While time-correlated single-photon counting (TCSPC) allows probing the dynamics of fluorescent photoexcited species, it is too slow for fast picosecond transitions along the S_1 PES and cannot monitor any dark states that may form. Therefore, we resorted to pump-probe transient-absorption TA spectroscopy to elucidate further the excited-state dynamics of these DPPs.

The TA spectra show the ground state bleach at 550–650 nm, modest stimulated emission at 695 nm, and the absorption of the singlet excited state of DPP at 750–800 nm (Figure 3a,c,e) [91–93]. In addition to these principal features that were to be expected for DPP conjugates, the evolution of the TA spectra revealed a subtle rise of absorption bands in the region around 550 to 650 nm (Figure 3a,c,e). This weak TA band at 640 nm became especially apparent for **13** at nanosecond probe delays (Figure 3c).

Global fit (GF) analysis revealed that, prior to the nanosecond decays that TCSPC showed, the three DPPs underwent picosecond transitions (Figure 3b,d,f). For **5**, the 10 ps transition led to shifts of some of the band and reshaping the TA spectra without significant change in the amplitudes (Figure 3b). The nanosecond decay led to a small TA band centered around 600 nm, indicating the formation of a transient with a lifetime quite longer than the dynamic range of the pump-probe technique, as represented by ΔA_{∞} (Figure 3b).

In contrast, a decrease of the TA amplitudes by about a factor of two reflected the picosecond transitions of the conjugates with thiophene moieties **13** and **15** (Figure 3d,f). Allowing $\Delta A_{\infty}(\lambda)$ to fluctuate for **13**, and setting $\Delta A_{\infty}(\lambda) = 0$ for **15**, aided the conversion of the GFs. That is, the nanosecond decay of **13** led to a long-lived transient, with TA peaking at about 645 nm (Figure 3d). While **15** also may form such a long-lived transient, its TA amplitudes were undetectable by the GF analysis.

The DPP radical anion had a pronounced TA band at around 640 nm [91,93]. Nevertheless, the triplets of different DPP conjugates also absorbed between about 600 and 650 nm [94,95]. Considering the picosecond intramolecular charge transfer (CT) of other DPP conjugates, followed by subnanosecond back CT [91–93], suggests that the transients revealed by $\Delta A_{\infty}(\lambda)$ formed too slowly and had too long lifetimes to have had originated from the radical anion of DPP. Therefore, the long-lived transients that **5** and **13** formed most plausibly indicates for triplet formation. The TA dynamics suggests that intersystem crossing (ISC) principally contributed to the deactivation of the excited states of **5** and **13**. In the excited-state dynamics of **15**, on the other hand, ISC did not play a key role.

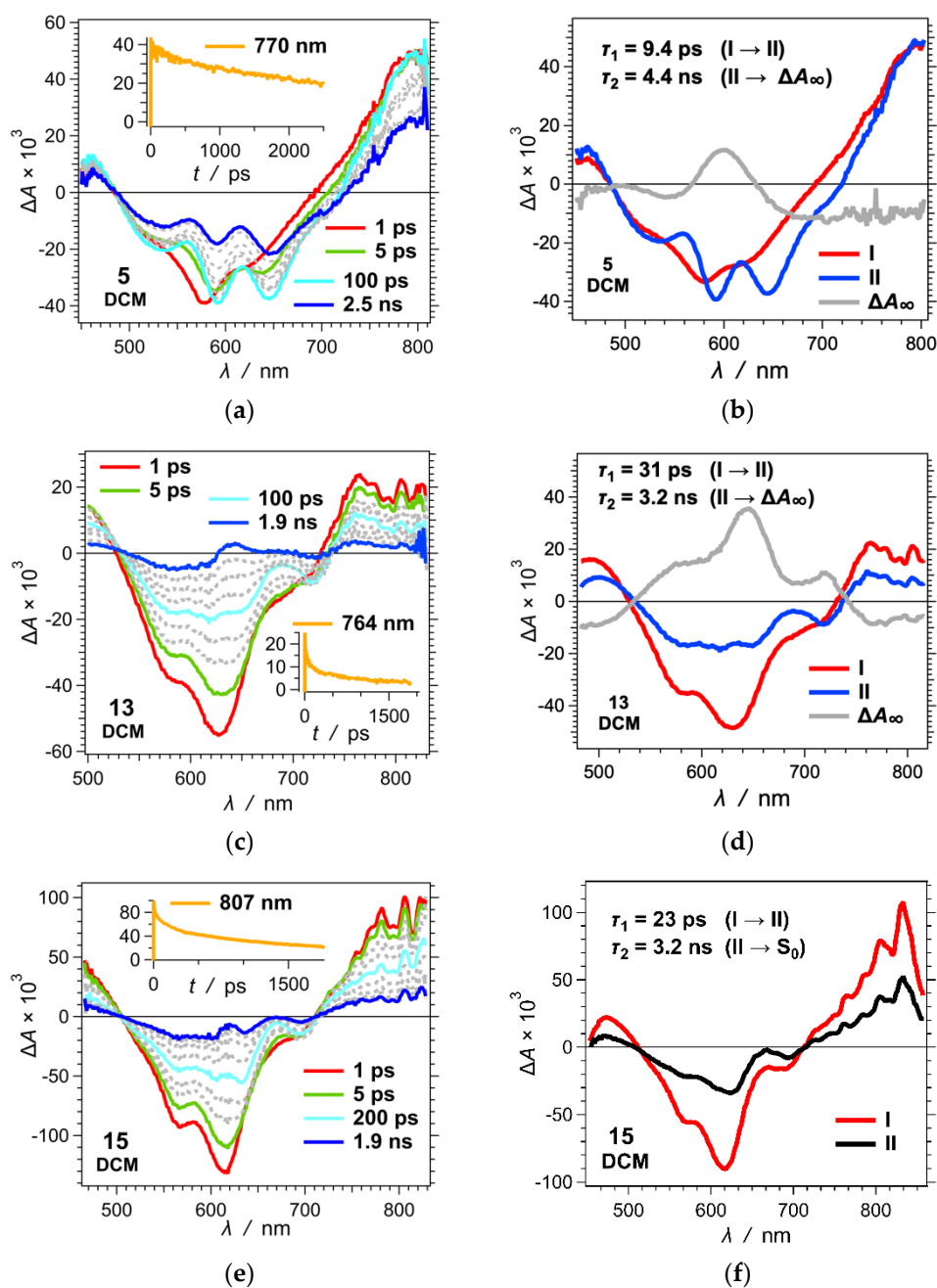


Figure 3. Transient-absorption dynamics of compounds **5**, **13**, and **15** for DCM. (a,c,e) Representative TA spectra of **5**, **13**, and **15** for DCM. Insets: the decays of the singlet excited states, $^1\text{DPP}^*$, of **5**, **13**, and **15** ($\lambda_{ex} = 400$ nm, $5 \mu\text{J}$ per pulse). (b,d,f) Spectra of **5**, **13**, and **15** for DCM, representing the transitions associated with each of the time constants, τ_i , obtained from the decay associated difference spectra, α_i vs. λ , that biexponential global fits produce, i.e., $\Delta A(\lambda, t) = \Delta A_\infty(\lambda) + \alpha_1(\lambda) \exp(-t/\tau_1) + \alpha_2(\lambda) \exp(-t/\tau_2)$. (I and II—transition spectra; ΔA_∞ —spectra of transients with lifetimes that considerably exceeds the dynamic range of the pump-probe technique; S_0 —ground state). The nanosecond time constants, τ_2 , are obtained from TCSPC and introduced as set parameters to the global fit analysis.

2.3. Theoretical Modelling

Time-dependent density-functional theory (TD-DFT) calculations allowed us to explore the structural and optical properties of the investigated dyes. The ground-state geometry of **5** showed the expected dihedral angles between the DPP core and the benzene rings (31°) and between these benzene rings and the benzothiazole moieties (39°), the presence of the methoxy substituents preventing planarity for the latter. There was a partial planarization in the lowest excited state with respective dihedrals of 20° and 19° ,

respectively. In contrast, **13** and **15** with the additional thienyl spacer allowed for a stronger π -conjugation, with dihedrals between the thienyl groups and the DPP core of 2° (1°) in the ground-state and 0° (1°) in the lowest excited-state. Nevertheless, the planarization of the benzene and benzoxazole upon going from the ground to the excited state pertained to both **13** and **15**, with, e.g., a thienyl-phenyl twist going from 26° to 4° in **13**.

Theory returned 0-0 wavelengths of 556, 646, and 629 nm for **5**, **13**, and **15** in DCM, respectively. These values compare favorably with the experimental position of the crossing point between the absorption/emission curves, i.e., 515, 631, and 620 nm (Figure 2). These results show that theory reproduced both quantitatively and qualitatively the experimental values. Electron density difference (EDD) plots provide representation of the transitions between the ground and excited states (Figure 4). The excited state was systematically localized on the DPP core with no significant CT character, which is consistent with the lack of solvent-polarity effects on the experimentally obtained absorption and emission maxima (Table 1). It further confirms that the long-lived transients of **5** and **13**, which their TA spectra revealed (Figure 3b,d), are their triplets, rather than long-lived CT states.

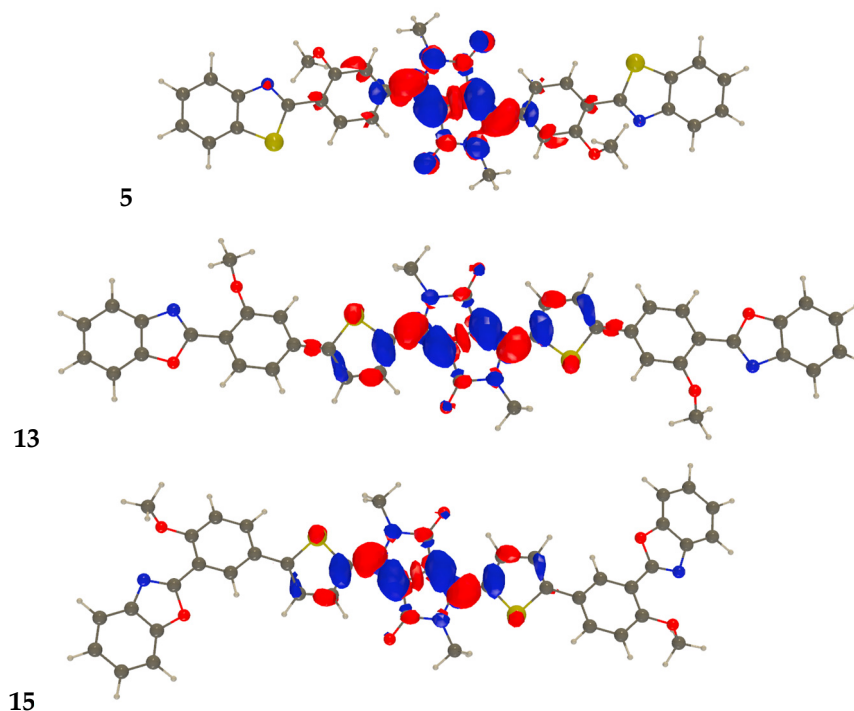


Figure 4. Density difference plots for the lowest absorption of (from top to bottom): **5**, **13**, and **15**. The crimson and blueberry regions indicate zones of increase and decrease of electronic density upon photoabsorption. A contour of 1×10^{-3} au is used.

Indeed, the amount of transferred charged q^{CT} amounted to ca. 0.3–0.4 e in all three dyes, clearly confirming the localized nature of the transition. Nevertheless, EDD of **5** indicates that the side benzene rings played a trifling role in the optical transitions (Figure 4). The EDDs of **13** and **15** on the other side, on the other hand, reveal that the thienyl moieties vicinal to the DPP core contributed to the optical transitions (Figure 4), which is consistent with their bathochromically shifted absorption (Figure 2, Table 1). This extension of the EDD was slightly more pronounced for the *para*-benzoxazole derivative, **13**, than with the *meta*-one, **15** (Figure 4), which agrees with what the absorption spectra show (Figure 2).

3. Discussion

The decrease in dihedral angle upon moving from phenyl substituents ($\sim 30^\circ$) to 5-membered rings ($\sim 7^\circ$) leads to significant changes in the photophysical properties of the re-

sultant *N,N*-dialkylDPPs, with an especially notable bathochromic shift in absorption [21–29]. The lower dihedral angle allows the substituent to have a greater contribution to the π -system of the DPP core in the ground state [21–29]. Our study corroborates these earlier observations, i.e., the replacement of 1,4-phenylene with a 2,5-thienylene as a linker directly attached to DPP core (**5** vs. **13**, **15**) leads to a 100 nm red-shift of both absorption and emission (Table 1). These properties resemble a DPP possessing two pyrene-2-yl-thienyl substituents [80]. This π -expansion leads to drastic decrease in the fluorescence quantum yields from what has been previously observed by Würthner and co-workers [79].

Moving the benzoxazole moiety from position 4 to position 3 of the benzene ring (**13**→**15**) slightly alters the photophysical properties of the resulting DPP. Both the absorption and emission of **15** are shifted hypsochromically (~10 nm), and increased radiative constants are observed in all solvents studied (Table 1).

4. Materials and Methods

All commercial materials (Sigma-Aldrich, Fluorochem, etc.) were used without further purification. All solvents were reagent or HPLC (Honeywell) grade. Unless otherwise noted, all reactions were run under argon atmosphere in flame-dried glassware. Reactions were stirred using Teflon-coated magnetic stir bars. TLC was performed on aluminium sheets, Merck 60F with fluorescent indicator F254 (Merck, Darmstadt, Germany). Plates were visualized by treatment with UV, acidic *p*-anisaldehyde stain, KMnO₄ stain, or aqueous ceric ammonium molybdate (Hanessian's stain; CAM) with gentle heating. Products were purified by flash column chromatography using the solvent systems indicated. Column chromatography was performed on Merck silica gel 60, 230–400 mesh.

All reported ¹H-NMR spectra were recorded using Bruker 400 MHz (Bruker BioSpin GmbH, Rheinstetten, Germany) or Varian 500 or 600 MHz (Agilent, Santa Clara, CA 95051, United States) spectrometers. Chemical shifts are quoted on the (δ ppm) scale, multiplicity (s = singlet, bs = broad singlet, d = doublet, t = triplet, q = quartet, m = multiplet), coupling constants are given in Hz. Solvent signal was indicated as the internal standard (CDCl₃, ¹H-NMR 7.26 ppm)¹ unless otherwise noted; *J* values are given in Hz. The mass spectra were obtained via electron ionization (EI-MS). Diketopyrrolopyrroles **12** and **14** were prepared following the literature procedure [96].

Steady-state absorption spectra were recorded in a transmission mode using a JASCO V-670 spectrophotometer (Jasco, Tokyo, Japan). The steady-state emission spectra and the time-correlated single-photon counting (TCSPC) fluorescence decays were measured using a FluoroLog-3 spectrofluorometer (Horiba-Jobin-Yvon, Edison, NJ, USA) equipped with a pulsed diode laser ($\lambda = 406$ nm, 196 ps pulse width) as previously reported. The wavelengths of the maxima of the absorption and emission spectra were obtained from fitting the spectra peaks with Gaussian function. For estimating zero-to-zero energy, E_{00} , of a conjugate, we plotted its absorption and fluorescence spectra on the same graph where the fluorescence maximum was adjusted to be equal to the maximum of the band at the red edge of the absorption spectrum. E_{00} was estimated from the wavelength at which the thus normalized spectra crossed. The fluorescence quantum yields, Φ_{fl} , were determined by comparing the integrated emission intensities of the samples with the integrated fluorescence of a reference sample with a known fluorescence quantum yield, where $F(\lambda)$ is the fluorescence intensity at wavelength λ ; $A(\lambda_{ex})$ is the absorbance at the excitation wavelength; n is the refractive index of the media; and the suffix "0" indicates the quantities for the reference sample used. For a reference sample we used an aqueous solution of fluorescein buffered at pH 10 ($\Phi_{fl} = 0.93$).

The transient-absorption (TA) data, $\Delta A(\lambda, t)$, were recorded in transmission mode with 2 mm quartz cuvettes using a Helios pump-probe spectrometer (Ultrafast Systems, LLC, Sarasota, FL, USA) equipped with a delay stage allowing maximum probe delays of 3.2 ns at 7 fs temporal step resolution [16]. Following chirp correction, we extracted the TA spectra and decays from $\Delta A(\lambda, t)$. The absorbance of the samples at the excitation wavelength, $A(\lambda_{ex})$, was adjusted to about 0.4 to 0.6 in the 2 mm cuvettes. Immediately

prior to the measurements, all samples were purged with argon for 5 to 10 min per 1 mL of sample. The photostability of the samples during the exposure to the pump laser was confirmed by comparing the absorption spectra recorded before and after each set of TA measurements. The laser source for the Helios was a SpitFire Pro 35F regenerative amplifier (Spectra Physics, Newport, CA, USA) generating 800 nm pulses (>35 fs, 4.0 mJ, at 1 kHz). The amplifier was pumped with of an Empower 30 Q-switched laser that ran at 20 W at the 2nd harmonic. A MaiTai SP oscillator provided the seed beam (55 nm bandwidth). The wavelength of the pump was tuned using an optical parametric amplifier, OPA-800CU (Newport Corporation, Newport, CA, USA), equipped with reflectors for removing the 800 nm fundamental and the signal, and the idler was subjected to second and fourth harmonic generators. For optimal OPA performance, the pulse duration from the amplifier was tuned to 50 fs. The idler was tuned in the range between 1840 and 1940 nm for selective excitation of DPP chromophore after upconversion to the fourth harmonic. The power of the signal and the idler removing the removal of the fundamental was stabilized at about 170 mW.

The fluorescence quantum yields, Φ_f , were estimated using fluorescein in aqueous alkaline solution as a standard:

$$\Phi_f/\Phi_f^{(0)} = (F/F^{(0)}) ((1 - 10^{-A(0)})/(1 - 10^{-A})) (n/n^{(0)})^2$$

where A is the absorbance (in the range of 0.01–0.15), F is the area under the curves of the emission spectra, n is the refractive index of the solvents (at 25 °C) used in measurements, and the superscripts (0) designates the standard. The following refractive index values were used: 1.424 for DCM, 1.344 for MeCN, 1.477 for DMSO, 1.362 for EtOH, 1.33 for aqueous 0.1 N NaOH.

3,6-Bis(4-bromo-3-methoxyphenyl)-2,5-dibutyl-2,5-dihydropyrrolo [3,4-c]pyrrole-1,4-dione (4). Sodium (0.92 g, 40.0 mmol), catalytic amount of FeCl₃, and *tert*-amylalcohol (20.0 mL) were added to a 100 mL dried flask at room temperature under argon gas. Then the reaction mixture was stirred for 2 h at 95 °C until sodium dissolved. After cooling the mixture to 60 °C, nitrile **1** (2.12 g, 10.0 mmol) was added in one portion, temperature was again raised up to 110 °C, and diisopropyl succinate (1.01 g, 5.0 mmol) dissolved in *tert*-amylalcohol (2 mL) was added dropwise during next hour. The mixture was heated to 110 °C and stirred at the temperature for 20 h. After cooling the mixture to 60 °C, acetic acid (2 mL) and methanol (40 mL) were added, and the mixture was stirred at 60 °C for 30 min, cooled to room temperature, and then poured into methanol (100 mL). Red insoluble precipitate was formed, filtered, and washed with fresh portion (50 mL) of cold MeOH. Crude material (1.66 g) was suspended in DMF 30 mL, K₂CO₃ (2.76 g, 20.0 mmol) was added in one portion, and reaction mixture was stirred in 50 °C for 2 h; next, 1-bromobutane (4.11 g, 30 mmol) was added. Temperature was increased to 70 °C, and the mixture was stirred overnight. Solvent was evaporated, and crude material was purified by flash column chromatography (silica gel, EtOAc/hexanes, 3:7) to give **4** as red shiny crystals 710 mg (23%). ¹H-NMR (400 MHz, CDCl₃) δ 7.67 (d, J = 8.2 Hz, 2H), 7.62 (d, J = 2.0 Hz, 2H), 7.17 (dd, J = 8.2, 2.0 Hz, 2H), 4.03 (s, 6H), 3.82–3.77 (m, 4H), 1.59 (quin, J = 7.6 Hz, 4H), 1.28–1.31 (m, 4H), 0.87 (t, J = 7.6 Hz, 6H). ¹³C-NMR (151 MHz, CDCl₃) δ 162.5, 156.3, 147.5, 133.6, 128.4, 120.9, 115.3, 112.8, 110.0, 56.6, 41.9, 31.6, 20.0, 13.6. HRMS (EI m/z): [M⁺] Calcd. for C₂₈H₃₀N₂O₄Br₂: 616.0572; found, 616.0564.

3,6-Bis(4-(benzo[d]thiazol-2-yl)-3-methoxyphenyl)-2,5-dibutyl-2,5-dihydropyrrolo [3,4-c]pyrrole-1,4-dione (5). A 50 mL Ace pressure vessel containing Ni(OAc)₂·4H₂O (249 mg, 1.0 mmol) was dried with a heat gun under vacuum and filled with argon after cooling to room temperature. To this vessel were added bipy (156 mg, 1.0 mmol), LiOt-Bu (24.0 mg, 0.30 mmol), compound **4** (61.8 mg, 0.10 mmol), and benzothiazole (40.6 mg, 0.30 mmol), followed by dry 1,4-dioxane (25 mL). The resulting mixture was heated at 95 °C for 16 h with stirring. After cooling to room temperature, solvent was evaporated and crude material was purified by flash column chromatography (silica gel, EtOAc/hexanes, 3:7) to give 35 mg (48%) of **5** as red shiny crystals. ¹H-NMR (500 MHz, CDCl₃) δ 8.47 (d, J = 8.3 Hz, 2H),

8.20 (d, $J = 8.3$ Hz, 2H), 8.08 (d, $J = 8.3$ Hz, 2H), 7.92 (s, 2H), 7.85 (t, $J = 7.8$ Hz, 2H), 7.76 (t, $J = 7.8$ Hz, 2H), 7.56 (d, $J = 7.9$ Hz, 2H), 4.32 (br s, 6H), 3.88–3.85 (m, 4H), 1.62–1.58 (m, 4H), 1.28–1.31 (m, 4H), 0.87 (t, $J = 7.6$ Hz, 6H). ^{13}C -NMR (126 MHz, CDCl_3) δ 166.3, 162.9, 158.6, 148.7, 139.6, 135.0, 130.7, 130.4, 129.9, 129.0, 122.5, 121.0, 118.2, 116.6, 113.8, 111.8, 57.2, 42.7, 31.4, 19.7, 13.2. HRMS (EI m/z): $[\text{M}^+\bullet]$ Calcd. for $\text{C}_{42}\text{H}_{38}\text{N}_4\text{O}_4\text{S}_2$: 726.2334; found, 726.2395.

2-(4-Bromo-2-methoxyphenyl)benzo[d]oxazole (7). Aldehyde **6** (3.46 g, 16.1 mmol), 2-aminophenol (1.93 g, 17.1 mmol), and NaCN (0.039 g, 0.804 mmol) were transferred to a 100 mL round-bottom flask. The reagents were dissolved in 60 mL of DMF, and an oxygen balloon was attached to the reaction mixture. The mixture was stirred at 50 °C for 4 h and monitored by TLC. Upon completion of the reaction, the mixture was evaporated, diluted with saturated Na_2CO_3 , and extracted with DCM ($3 \times 25\text{mL}$). The organic layer was dried over Na_2SO_4 and concentrated. The product was purified using flash column chromatography (silica gel, EtOAc/hexanes, from 1:19 to 1:9). The product was recrystallized from cold EtOH to afford 3.33 g (68%) of compound **7** as light-yellow needles. ^1H -NMR (600 MHz, CDCl_3) δ 8.28 (d, $J = 2.6$ Hz, 1H), 7.85–7.79 (m, 1H), 7.61–7.57 (m, 2H), 7.38–7.35 (m, 2H), 6.97 (d, $J = 8.9$ Hz, 1H), 4.01 (s, 3H). ^{13}C -NMR (151 MHz, CDCl_3) δ 160.0, 157.5, 150.3, 141.9, 135.2, 133.6, 125.3, 124.5, 120.4, 117.9, 113.9, 112.8, 110.5, 56.5. HRMS (EI m/z): $[\text{M}^+\bullet]$ Calcd. for $\text{C}_{14}\text{H}_{10}\text{BrNO}_2$: 302.9895; found, 302.9889.

2-(2-Methoxy-4-(4,4,5,5-tetramethyl-1,3,2-dioxaborolan-2-yl)phenyl)benzo[d]oxazole (8). Compound **7** (502 mg, 1.65 mmol), bis(pinacolato)diboron (461 mg, 1.81 mmol) and potassium acetate (486 mg, 1.81 mmol) in 20 mL of 1,4-dioxane were placed in a dry, argon-purged Schlenk tube. Next, Pd(dppf) Cl_2 was added to the mixture, heated to 100 °C, and stirred overnight. The mixture was quenched with EtOAc and filtered through short pad of Celite. The product was purified using flash column chromatography (silica gel; EtOAc/hexanes, 2:3) and recrystallized from cold EtOH to afford 463 mg (80%) of compound **8** as light-yellow needles. ^1H -NMR (400 MHz, CDCl_3) δ 8.15 (d, $J = 7.7$ Hz, 1H), 7.86–7.80 (m, 1H), 7.62–7.57 (m, 1H), 7.54 (d, $J = 7.7$ Hz, 1H), 7.50 (s, 1H), 7.38–7.30 (m, 2H), 4.07 (s, 3H), 1.37 (s, 12H). ^{13}C -NMR (101 MHz, CDCl_3) δ 161.5, 157.7, 150.4, 142.2, 130.4, 127.0, 125.0, 124.3, 120.3, 118.5, 117.7, 110.5, 84.2, 56.3, 24.9. HRMS (EI m/z): $[\text{M}^+\bullet]$ Calcd. for $\text{C}_{20}\text{H}_{22}\text{BNO}_4$: 351.1642; found, 351.1648.

2-(5-Bromo-2-methoxyphenyl)benzo[d]oxazole (10). Compound **9** (2.00 g, 9.3 mmol), 2-aminophenol (1.68 g, 15.3 mmol), and NaCN (0.022 g, 0.465 mmol) were transferred to a 100 mL round-bottom flask. The reagents were dissolved in 40 mL of DMF. An oxygen balloon was attached, and the reaction mixture was stirred at 110 °C for 2 h. Upon completion of the reaction, the volatiles were evaporated. The product was purified using flash column chromatography (silica gel; EtOAc/hexanes, 3:17) and recrystallized from cold EtOH to afford 1.94 g (68%) of compound **10** as light-yellow needles. ^1H -NMR (600 MHz, CDCl_3) δ 8.28 (d, $J = 2.6$ Hz, 1H), 7.83 (ddd, $J = 5.7, 2.2, 0.7$ Hz, 1H), 7.63–7.56 (m, 2H), 7.42–7.32 (m, 2H), 6.98 (d, $J = 8.9$ Hz, 1H), 4.01 (s, 3H). ^{13}C -NMR (151 MHz, CDCl_3) δ 160.0, 157.5, 150.3, 141.8, 135.3, 133.6, 125.4, 124.5, 120.4, 117.9, 113.9, 112.8, 110.5, 56.5. HRMS (EI m/z): $[\text{M}^+\bullet]$ Calcd. for $\text{C}_{14}\text{H}_{10}\text{BrNO}_2$: 302.9895; found, 302.9904.

2-(2-Methoxy-5-(4,4,5,5-tetramethyl-1,3,2-dioxaborolan-2-yl)phenyl)benzo[d]oxazole (11). Compound **10** (502 mg, 1.65 mmol), bis(pinacolato)diboron (461 mg, 1.81 mmol), and potassium acetate (486 mg, 1.81 mmol) in 20 mL of 1,4-dioxane were placed into a dry, argon-purged Schlenk tube. Next, Pd(dppf) Cl_2 was added to the mixture and was heated at 100 °C overnight. After completion of the reaction, it was quenched with EtOAc and filtered through short pad of Celite. The product was purified using flash column chromatography (silica gel; EtOAc/hexanes, 3:7) and recrystallized from cold EtOH to afford 475 mg (82%) of compound **11** as light-yellow needles. ^1H -NMR (600 MHz, CDCl_3) δ 8.58 (d, $J = 1.7$ Hz, 1H), 7.95 (dd, $J = 8.4, 1.7$ Hz, 1H), 7.86–7.80 (m, 1H), 7.62–7.57 (m, 1H), 7.37–7.31 (m, 2H), 7.08 (d, $J = 8.4$ Hz, 1H), 4.05 (s, 3H), 1.36 (s, 12H). ^{13}C -NMR (151 MHz, CDCl_3) δ 161.4, 160.8, 150.2, 142.1, 139.6, 138.1, 124.9, 124.2, 120.2, 115.6, 111.3, 110.4, 83.9, 75.0, 56.2, 24.9. HRMS (EI m/z): $[\text{M}^+\bullet]$ Calcd. for $\text{C}_{20}\text{H}_{22}\text{BNO}_4$: 351.1642; found, 351.1649.

3,6-Bis(5-(4-(benzo[d]oxazol-2-yl)-3-methoxyphenyl)thiophen-2-yl)-2,5-dihexylpyrrolo[3,4-c]pyrrole-1,4(2H,5H)-dione (**13**). Compound **12** (187 mg, 0.40 mmol), aryl bromide **7** (280 mg, 0.92 mmol), palladium (II) acetate (5.0 mg, 5 mol%), and potassium acetate (86 mg, 0.88 mmol) were placed in a dry, argon-purged Schlenk tube. DMA (3 mL) was added, and the suspension was degassed 3 times by evacuation, and the Schlenk tube was refilled with argon gas. The mixture was heated at 150 °C overnight. The product was purified using flash column chromatography (silica gel; with gradient from CHCl₃ to CHCl₃/EtOAc, 1:4) and recrystallized from EtOAc to afford 120 mg (33%) of **13** as violet shiny crystals. ¹H-NMR (500 MHz, CDCl₃ + TFA-*d*₁) δ 8.78 (br s, 2H), 8.53 (br s, 2H), 8.08 (d, *J* = 11.9 Hz, 2H), 7.96 (d, *J* = 9.1 Hz, 2H), 7.87 (d, *J* = 8.9, 2H), 7.74–7.65 (m, 4H), 7.58 (d, *J* = 4.1 Hz, 2H), 7.33 (d, *J* = 8.9 Hz, 2H), 4.19 (s, 6H), 4.17–4.12 (m, 4H), 1.86–1.76 (m, 4H), 1.51–1.43 (m, 4H), 1.41–1.32 (m, 8H), 0.91 (t, *J* = 6.9 Hz, 6H). ¹³C-NMR (126 MHz, CDCl₃) δ 162.1, 160.8, 160.2, 147.7, 147.6, 143.2, 141.2, 137.0, 131.7, 131.2, 129.4, 129.1, 128.5, 120.0, 116.0, 112.2, 110.0, 109.4, 109.3, 107.2, 57.0, 43.0, 31.2, 29.7, 26.4, 22.4, 13.8. HRMS (EI *m/z*): [M⁺•] Calcd. for C₅₄H₅₀N₄O₆S₂: 914.3172; found, 914.3168.

3,6-Bis(5-(3-(benzo[d]oxazol-2-yl)-4-methoxyphenyl)thiophen-2-yl)-2,5-dihexylpyrrolo[3,4-c]pyrrole-1,4(2H,5H)-dione (**15**). Dye **11** (176 mg, 0.5 mmol), compound **14** (76 mg, 0.25 mmol), Cs₂CO₃ (489 mg, 1.5 mmol), and Pd(dppf)Cl₂ (18.3 mg, 0.025 mmol) were suspended in a dry toluene (2 mL) in an argon-purged Schlenk tube. The mixture was heated at 107 °C overnight. The reaction mixture was concentrated, and the product was purified by flash column chromatography (silica gel; with gradient: from CHCl₃ to CHCl₃/EtOAc, 1:4). The product was recrystallized from MeOH to afford 55 mg (24%) of **15** as dark purple solid. ¹H-NMR (500 MHz, CDCl₃) δ 8.70 (d, *J* = 4.0 Hz, 2H), 8.59 (d, *J* = 2.4 Hz, 2H), 8.15 (m, 2H), 7.92 (m, 4H), 7.77 (m, 4H), 7.63 (d, *J* = 4.0 Hz, 2H), 7.39 (d, *J* = 8.9 Hz, 2H), 4.23 (s, 6H), 4.15 (t, *J* = 8.0 Hz, 4H), 1.82 (quin, *J* = 7.9 Hz, 4H), 1.48 (quin, *J* = 7.4, 4H), 1.42–1.32 (m, 8H), 0.91 (t, *J* = 6.9 Hz, 6H). ¹³C-NMR (126 MHz, CDCl₃) δ 162.1, 160.5, 160.1, 147.9, 147.7, 141.3, 137.2, 136.9, 129.7, 129.2, 128.8, 128.5, 127.9, 127.6, 126.0, 116.4, 113.9, 112.2, 108.4 (2 signals), 57.3, 31.3, 29.7, 29.7, 26.4, 22.5, 13.9. HRMS (EI *m/z*): [M⁺•] Calcd. for C₅₄H₅₀N₄O₆S₂: 914.3172; found, 914.3146.

All density functional theory (DFT) and time-dependent DFT (TD-DFT) calculations were carried out with the Gaussian 16 package [97]. The integral equation formalism (IEF) version of the polarizable continuum (PCM) model was used to include the solvent effects, considering DCM ($\epsilon = 8.93$) as medium. The ground state geometries of **5**, **13**, and **15** were first fully optimized using the M06-2X [98] exchange-correlation functional with the 6-311G(d,p) atomic basis set. Next, frequency calculations were performed at the same level of theory to ensure that each optimized structure was a true minimum on the potential energy surface (absence of imaginary frequency). The geometries of the lowest electronic excited states of the three DPP dyes were similarly obtained at the TD-M06-2X/6-311G(d,p) level of theory, and analytic frequency calculations were also done at the same level to check that their excited states structures were true minima of the excited state potential energy surface. From the optimal equilibrium geometries, the vertical transition energies were calculated using the same hybrid functional but a larger basis set—namely, 6-311+G(2d,p). The solvent effects were accounted for using the linear-response PCM model, adequate for bright transitions.

5. Conclusions

There are multiple implications of the results of this study. The synthesis of 2,5-diaryl-diketopyrrolopyrroles, possessing complex substituents, could be realized with the help of direct arylation. The presence of thiophene moiety directly linked with diketopyrrolopyrrole core enables a significant bathochromic shift of both absorption and emission. The presence of substituents fails to impose any charge-transfer character on the S₁ state. The peripheral aryl substituents are inactive in the S₀→S₁ transition, resulting in a small influence on the type of substitution of the photophysical properties. Finally, shifting the benzoxazole moiety in diketopyrrolopyrroles changes the principal deactivation path-

way, with intersystem crossing prevailing when all units are bridged in *para* positions. These findings may serve as a blueprint to design diketopyrrolopyrroles with fine-tuned optical properties.

Supplementary Materials: The following are available online. Figure S1: ^1H and ^{13}C -NMR spectral data for **4**, Figure S2: ^1H and ^{13}C -NMR spectral data for **5**, Figure S3: ^1H and ^{13}C -NMR spectral data for **7**, Figure S4: ^1H and ^{13}C -NMR spectral data for **8**, Figure S5: ^1H and ^{13}C -NMR spectral data for **10**, Figure S6: ^1H and ^{13}C -NMR spectral data for **11**, Figure S7: ^1H and ^{13}C -NMR spectral data for **13**, Figure S8: ^1H and ^{13}C -NMR spectral data for **15**, Figure S9: Absorption and emission spectra of DPPs **5**, **13** and **15** in toluene, Figure S10: Absorption and emission spectra of DPPs **5**, **13** and **15** in DMF.

Author Contributions: Conceptualization, D.T.G.; formal analysis, J.B.D.; investigation, M.P., J.B.D., A.C., O.V., and J.A.C.; writing—original draft preparation, D.T.G., M.P., J.B.D., D.J., and B.K.; writing—review and editing, D.T.G., V.I.V., and D.J.; visualization, M.P. and J.B.D.; supervision, D.T.G., V.I.V., and D.J. All authors have read and agreed to the published version of the manuscript.

Funding: This research was funded by the Foundation for Polish Science (POIR.04.04.00-00-3CF4/16-00), the U.S.A. National Science Foundation (NSF, grants CHE 1465284 and CBET 0923408). D.J. acknowledges the Region des Pays de la Loire for constant support. This work used computational resources from the CCIPL, the CINES, and the local Troy cluster.

Institutional Review Board Statement: Not applicable.

Informed Consent Statement: Not applicable.

Data Availability Statement: The data presented in this study are available in this article and accompanying supplementary material.

Conflicts of Interest: The authors declare no conflict of interest. The funders had no role in the design of the study; in the collection, analyses, or interpretation of data; in the writing of the manuscript; or in the decision to publish the results.

Sample Availability: Samples of the compounds **5**, **13**, and **15** are available from the authors.

References

1. Barzoukas, M.; Blanchard-Desce, M. Molecular engineering of push–pull dipolar and quadrupolar molecules for two-photon absorption: A multivalence-bond states approach. *J. Chem. Phys.* **2000**, *113*, 3951–3959. [[CrossRef](#)]
2. Drobizhev, M.; Karotki, A.; Dzenis, Y.; Rebane, A.; Suo, Z.; Spangler, C.W. Strong Cooperative Enhancement of Two-Photon Absorption in Dendrimers. *J. Phys. Chem. B* **2003**, *107*, 7540–7543. [[CrossRef](#)]
3. Meier, H. Conjugated Oligomers with Terminal Donor–Acceptor Substitution. *Angew. Chem. Int. Ed.* **2005**, *44*, 2482–2506. [[CrossRef](#)] [[PubMed](#)]
4. Charlot, M.; Porrès, L.; Entwistle, C.D.; Beeby, A.; Marder, T.; Blanchard-Desce, M. Investigation of two-photon absorption behavior in symmetrical acceptor– π –acceptor derivatives with dimesitylboryl end-groups. Evidence of new engineering routes for TPA/transparency trade-off optimization. *Phys. Chem. Chem. Phys.* **2005**, *7*, 600–606. [[CrossRef](#)]
5. Charlot, M.; Izard, N.; Mongin, O.; Riehl, D.; Blanchard-Desce, M. Optical limiting with soluble two-photon absorbing quadrupoles: Structure–property relationships. *Chem. Phys. Lett.* **2006**, *417*, 297–302. [[CrossRef](#)]
6. Niko, Y.; Moritomo, H.; Sugihara, H.; Suzuki, Y.; Kawamata, J.; Konishi, G.-I. A novel pyrene-based two-photon active fluorescent dye efficiently excited and emitting in the ‘tissue optical window (650–1100 nm)’. *J. Mater. Chem. B* **2015**, *3*, 184–190. [[CrossRef](#)]
7. Tasiar, M.; Bald, I.; Deperasińska, I.; Cywiński, P.J.; Gryko, D.T. An internal charge transfer-dependent solvent effect in V-shaped azacyanines. *Org. Biomol. Chem.* **2015**, *13*, 11714–11720. [[CrossRef](#)]
8. Dereka, B.; Rosspointner, A.; Li, Z.; Liska, R.; Vauthey, E. Direct visualization of excited-state symmetry breaking using ultra-fast time-resolved infrared spectroscopy. *J. Am. Chem. Soc.* **2016**, *138*, 4643–4649. [[CrossRef](#)]
9. Liu, Z.-Q.; Fang, Q.; Cao, D.-X.; Wang, D.; Xu, G.-B. Triaryl Boron-Based A- π -A vs Triaryl Nitrogen-Based D- π -D Quadrupolar Compounds for Single- and Two-Photon Excited Fluorescence. *Org. Lett.* **2004**, *6*, 2933–2936. [[CrossRef](#)]
10. Parent, M.; Mongin, O.; Kamada, K.; Katan, C.; Blanchard-Desce, M. New chromophores from click chemistry for two-photon absorption and tuneable photoluminescence. *Chem. Commun.* **2005**, 2029–2031. [[CrossRef](#)]
11. Kim, H.M.; Yang, W.J.; Kim, C.H.; Park, W.-H.; Jeon, S.-J.; Cho, B.R. Two-Photon Dyes Containing Heterocyclic Rings with Enhanced Photostability. *Chem. A Eur. J.* **2005**, *11*, 6386–6391. [[CrossRef](#)]
12. Porrès, L.; Mongin, O.; Blanchard-Desce, M. Synthesis, fluorescence and two-photon absorption properties of multichromophoric boron-dipyrromethene fluorophores for two-photon-excited fluorescence applications. *Tetrahedron Lett.* **2006**, *47*, 1913–1917. [[CrossRef](#)]

13. Lin, T.-C.; Liu, Y.-Y.; Li, M.-H.; Liu, C.-Y.; Tseng, S.-Y.; Wang, Y.-T.; Tseng, Y.-H.; Chu, H.-H.; Luo, C.-W. Synthesis and Characterization of Two-Photon Chromophores Based on a Tetrasubstituted Tetraethynylethylene Scaffold. *Chem. Asian J.* **2014**, *9*, 1601–1610. [[CrossRef](#)] [[PubMed](#)]
14. Krzeszewski, M.; Thorsted, B.; Brewer, J.; Gryko, D.T. Tetraaryl-, Pentaaryl-, and Hexaaryl-1,4-dihydropyrrolo[3,2-b]pyrroles: Synthesis and Optical Properties. *J. Org. Chem.* **2014**, *79*, 3119–3128. [[CrossRef](#)] [[PubMed](#)]
15. Doval, D.A.; Molin, M.D.; Ward, S.; Fin, A.; Sakai, N.; Matile, S. Planarizable push–pull oligothiophenes: In search of the perfect twist. *Chem. Sci.* **2014**, *5*, 2819–2825. [[CrossRef](#)]
16. Fin, A.; Jentzsch, A.V.; Sakai, N.; Matile, S. Oligothiophene Amphiphiles as Planarizable and Polarizable Fluorescent Membrane Probes. *Angew. Chem.* **2012**, *124*, 12908–12911. [[CrossRef](#)]
17. Molin, M.D.; Matile, S. 3,4-Ethylenedioxythiophene in planarizable push–pull oligothiophenes. *Org. Biomol. Chem.* **2013**, *11*, 1952–1957. [[CrossRef](#)]
18. Doval, D.A.; Matile, S. Increasingly twisted push–pull oligothiophenes and their planarization in confined space. *Org. Biomol. Chem.* **2013**, *11*, 7467. [[CrossRef](#)]
19. Molin, M.D.; Verolet, Q.; Soleimanpour, S.; Matile, S. Mechanosensitive Membrane Probes. *Chem. A Eur. J.* **2015**, *21*, 6012–6021. [[CrossRef](#)]
20. Molin, M.D.; Verolet, Q.; Colom, A.; Letrun, R.; Derivery, E.; Gonzalez-Gaitan, M.; Vauthey, E.; Roux, A.; Sakai, N.; Matile, S. Fluorescent Flippers for Mechanosensitive Membrane Probes. *J. Am. Chem. Soc.* **2015**, *137*, 568–571. [[CrossRef](#)]
21. Grzybowski, M.; Gryko, D.T. Diketopyrrolopyrroles: Synthesis, Reactivity, and Optical Properties. *Adv. Opt. Mater.* **2015**, *3*, 280–320. [[CrossRef](#)]
22. Qu, S.; Qin, C.; Islam, A.; Wu, Y.; Zhu, W.; Hua, J.; Tian, H.; Han, L. A novel D–A– π -A organic sensitizer containing a diketopyrrolopyrrole unit with a branched alkyl chain for highly efficient and stable dye-sensitized solar cells. *Chem. Commun.* **2012**, *48*, 6972–6974. [[CrossRef](#)] [[PubMed](#)]
23. Qu, S.; Tian, H. Diketopyrrolopyrrole (DPP)-based materials for organic photovoltaics. *Chem. Commun.* **2012**, *48*, 3039–3051. [[CrossRef](#)]
24. Nielsen, C.B.; Turbiez, M.; McCulloch, I. Recent Advances in the Development of Semiconducting DPP-Containing Polymers for Transistor Applications. *Adv. Mater.* **2013**, *25*, 1859–1880. [[CrossRef](#)] [[PubMed](#)]
25. Liu, S.-Y.; Shi, M.-M.; Huang, J.-C.; Jin, Z.-N.; Hu, X.-L.; Pan, J.-Y.; Li, H.-Y.; Jen, A.K.-Y.; Chen, H.-Z. C–H activation: Making diketopyrrolopyrrole derivatives easily accessible. *J. Mater. Chem. A* **2013**, *1*, 2795. [[CrossRef](#)]
26. Jeong, Y.; Lee, C.; Jang, W. A Diketopyrrolopyrrole-Based Colorimetric and Fluorescent Probe for Cyanide Detection. *Chem. Asian J.* **2012**, *7*, 1562–1566. [[CrossRef](#)]
27. Guo, E.Q.; Ren, P.H.; Zhang, Y.L.; Zhang, H.C.; Yang, W.J. Diphenylamine end-capped 1,4-diketo-3,6-diphenylpyrrolo[3,4-c]pyrrole (DPP) derivatives with large two-photon absorption cross-sections and strong two-photon excitation red fluorescence. *Chem. Commun.* **2009**, 5859–5861. [[CrossRef](#)] [[PubMed](#)]
28. Humphreys, J.; Pop, F.; Hume, P.A.; Murphy, A.S.; Lewis, W.; Davies, E.S.; Argent, S.P.; Amabilino, D.B. Solid state structure and properties of phenyl diketopyrrolopyrrole derivatives. *CrystEngComm* **2021**, *23*, 1796–1814. [[CrossRef](#)]
29. Pop, F.; Humphreys, J.; Schwarz, J.; Brown, L.; Berg, A.V.D.; Amabilino, D.B. Towards more sustainable synthesis of diketopyrrolopyrroles. *New J. Chem.* **2019**, *43*, 5783–5790. [[CrossRef](#)]
30. Rochat, A.C.; Cassar, L.; Iqbal, A. Preparation of pyrrolo-(3,4-c) pyrroles. *Eur. Pat. Appl.* **1983**. EP 0094911 A3.
31. Iqbal, A.; Jost, M.; Kirchmayr, R.; Pfenninger, J.; Rochat, A.; Wallquist, O. The synthesis and properties of 1,4-diketo-pyrrolo [3,4-C] pyrroles. *Bull. Soc. Chim. Belg.* **1988**, *97*, 615–644. [[CrossRef](#)]
32. Hao, Z.; Iqbal, A. Some aspects of organic pigments. *Chem. Soc. Rev.* **1997**, *26*, 203–213. [[CrossRef](#)]
33. Zambounis, J.S.; Hao, Z.; Iqbal, A. Latent pigments activated by heat. *Nat. Cell Biol.* **1997**, *388*, 131–132. [[CrossRef](#)]
34. Wallquist, O.; Lenz, R. 20 years of DPP pigments—Future perspectives. *Macromol. Symp.* **2002**, *187*, 617–630. [[CrossRef](#)]
35. Iqbal, A.; Cassar, L.; Rochat, A.C.; Pfenninger, J.; Wallquist, O. Newheterocyclic pigments. *J. Coat. Technol.* **1988**, *60*, 37–45.
36. Farnum, D.G.; Mehta, G.; Moore, G.G.; Siegal, F.P. Attempted reformatskii reaction of benzonitrile, 1,4-diketo-3,6-diphenylpyrrolo[3,4-C]pyrrole. A lactam analogue of pentalene. *Tetrahedron Lett.* **1974**, *15*, 2549–2552. [[CrossRef](#)]
37. Pieczykolan, M.; Sadowski, B.; Gryko, D.T. An Efficient Method for the Programmed Synthesis of Multifunctional Diketopyrrolopyrroles. *Angew. Chem.* **2020**, *132*, 7598–7605. [[CrossRef](#)]
38. Alam, M.M.; Bolze, F.; Daniel, C.; Flamigni, L.; Gourlaouen, C.; Heitz, V.; Jenni, S.; Schmitt, J.; Sour, A.; Ventura, B. π -Extended diketopyrrolopyrrole–porphyrin arrays: One- and two-photon photophysical investigations and theoretical studies. *Phys. Chem. Chem. Phys.* **2016**, *18*, 21954–21965. [[CrossRef](#)]
39. Ftouni, H.; Bolze, F.; De Rocquigny, H.; Nicoud, J.-F. Functionalized Two-Photon Absorbing Diketopyrrolopyrrole-Based Fluorophores for Living Cells Fluorescent Microscopy. *Bioconjugate Chem.* **2013**, *24*, 942–950. [[CrossRef](#)]
40. Grzybowski, M.; Hugues, V.; Blanchard-Desce, M.; Gryko, D.T. Two-Photon-Induced Fluorescence in New π -Expanded Diketopyrrolopyrroles. *Chem. Eur. J.* **2014**, *20*, 12493–12501. [[CrossRef](#)] [[PubMed](#)]
41. He, T.; Gao, Y.; Sreejith, S.; Tian, X.; Liu, L.; Wang, Y.; Joshi, H.; Phua, S.Z.F.; Yao, S.; Lin, X.; et al. Biocompatible Two-Photon Absorbing Dipyrrolopyrroles for Metal-Ion-Mediated Self-Assembly Modulation and Fluorescence Imaging. *Adv. Opt. Mater.* **2016**, *4*, 746–755. [[CrossRef](#)]

42. Grzybowski, M.; Glodkowska-Mrowka, E.; Hugues, V.; Brutkowski, W.; Blanchard-Desce, M.; Gryko, D.T. Polar Diketopyrrolopyrrole-Imidazolium Salts as Selective Probes for Staining Mitochondria in Two-Photon Fluorescence Microscopy. *Chem. A Eur. J.* **2015**, *21*, 9101–9110. [[CrossRef](#)] [[PubMed](#)]
43. Purc, A.; Sobczyk, K.; Sakagami, Y.; Ando, A.; Kamada, K.; Gryko, D.T. Strategy towards large two-photon absorption cross-sections for diketopyrrolopyrroles. *J. Mater. Chem. C* **2015**, *3*, 742–749. [[CrossRef](#)]
44. Heath-Apostolopoulos, I.; Vargas-Ortiz, D.; Wilbraham, L.; Jelfs, K.E.; Zwijnenburg, M.A. Using high-throughput virtual screening to explore the optoelectronic property space of organic dyes; finding diketopyrrolopyrrole dyes for dye-sensitized water splitting and solar cells. *Sustain. Energy Fuels* **2021**, *5*, 704–719. [[CrossRef](#)]
45. Purc, A.; Koszarna, B.; Iachina, I.; Friese, D.H.; Tasiior, M.; Sobczyk, K.; Pędziński, T.; Brewer, J.; Gryko, D.T. The impact of interplay between electronic and steric effects on the synthesis and the linear and non-linear optical properties of diketopyrrolopyrrole bearing benzofuran moieties. *Org. Chem. Front.* **2017**, *4*, 724–736. [[CrossRef](#)]
46. Punzi, A.; Nicoletta, F.; Marzano, G.; Fortuna, C.G.; Dagar, J.; Brown, T.M.; Farinola, G.M. Synthetic Routes to TEG-Substituted Diketopyrrolopyrrole-Based Low Band-Gap Polymers. *Eur. J. Org. Chem.* **2016**, *2016*, 3233–3242. [[CrossRef](#)]
47. Stolte, M.; Suraru, S.-L.; Diemer, P.; He, T.; Burschka, C.; Zschieschang, U.; Klauk, H.; Würthner, F. Diketopyrrolopyrrole Organic Thin-Film Transistors: Impact of Alkyl Substituents and Tolerance of Ethylhexyl Stereoisomers. *Adv. Funct. Mater.* **2016**, *26*, 7415–7422. [[CrossRef](#)]
48. Tang, A.; Zhan, C.; Yao, J.; Zhou, E. Design of Diketopyrrolopyrrole (DPP)-Based Small Molecules for Organic-Solar-Cell Applications. *Adv. Mater.* **2017**, *29*, 1600013. [[CrossRef](#)]
49. Zhao, C.; Guo, Y.; Zhang, Y.; Yan, N.; You, S.; Li, W. Diketopyrrolopyrrole-based conjugated materials for non-fullerene organic solar cells. *J. Mater. Chem. A* **2019**, *7*, 10174–10199. [[CrossRef](#)]
50. Patil, Y.; Jadhav, T.; Dhokale, B.; Misra, R. Design and Synthesis of Low HOMO-LUMO Gap N-Phenylcarbazole-Substituted Diketopyrrolopyrroles. *Asian J. Org. Chem.* **2016**, *5*, 1008–1014. [[CrossRef](#)]
51. Lo, C.K.; Reynolds, J.R. Structural and morphological effects of alkyl side chains on flanking thiophenes of diketopyrrolopyrrole polymers for organic photovoltaic devices. *Polymer* **2016**, *99*, 741–747. [[CrossRef](#)]
52. Tieke, B.; Rabindranath, A.R.; Zhang, K.A.I.; Zhu, Y. Conjugated polymers containing diketopyrrolopyrrole units in the main chain. *Beilstein J. Org. Chem.* **2010**, *6*, 830–845. [[CrossRef](#)]
53. Wienk, M.M.; Turbiez, M.; Gilot, J.; Janssen, R.A.J. Narrow-bandgap diketo-pyrrolo-pyrrole polymer solar cells: The effect of processing on the performance. *Adv. Mater.* **2008**, *20*, 2556–2560. [[CrossRef](#)]
54. Kanibolotsky, A.L.; Vilela, F.; Forgie, J.C.; Elmasly, S.E.T.; Skabara, P.J.; Zhang, K.A.I.; Tieke, B.; McGurk, J.; Belton, C.R.; Stavrinou, P.N.; et al. Well-Defined and Monodisperse Linear and Star-Shaped Quaterfluorene-DPP Molecules: The Significance of Conjugation and Dimensionality. *Adv. Mater.* **2011**, *23*, 2093–2097. [[CrossRef](#)]
55. Li, Y.; Sonar, P.; Murphy, L.; Hong, W. High mobility diketopyrrolopyrrole (DPP)-based organic semiconductor materials for organic thin film transistors and photovoltaics. *Energy Environ. Sci.* **2013**, *6*, 1684–1710. [[CrossRef](#)]
56. Hendriks, K.H.; Heintges, G.H.L.; Gevaerts, V.S.; Wienk, M.M.; Janssen, R.A.J. High-Molecular-Weight Regular Alternating Diketopyrrolopyrrole-based Terpolymers for Efficient Organic Solar Cells. *Angew. Chem. Int. Ed.* **2013**, *52*, 8341–8344. [[CrossRef](#)]
57. Coffin, R.C.; Peet, J.; Rogers, J.; Bazan, G.C.; Peet, R. Streamlined microwave-assisted preparation of narrow-bandgap conjugated polymers for high-performance bulk heterojunction solar cells. *Nat. Chem.* **2009**, *1*, 657–661. [[CrossRef](#)]
58. Li, Y.; Sonar, P.; Singh, S.P.; Ooi, Z.E.; Lek, E.S.H.; Loh, M.Q.Y. Poly (2, 5-bis (2-octyldodecyl)-3, 6-di (furan-2-yl)-2, 5-dihydro-pyrrolo [3, 4-c] pyrrole-1, 4-dione-co-thieno [3, 2-b] thiophene): A high performance polymer semiconductor for both organic thin film transistors and organic photovoltaics. *Phys. Chem. Chem. Phys.* **2012**, *14*, 7162–7169. [[CrossRef](#)]
59. Sonar, P.; Singh, S.P.; Williams, E.L.; Li, Y.; Soh, M.S.; Dodabalapur, A. Furan containing diketopyrrolopyrrole copolymers: Synthesis, characterization, organic field effect transistor performance and photovoltaic properties. *J. Mater. Chem.* **2012**, *22*, 4425–4435. [[CrossRef](#)]
60. Murphy, A.S.; Killalea, C.E.; Humphreys, J.; Hume, P.A.; Cliffe, M.J.; Murray, G.J.; Davies, E.S.; Lewis, W.; Amabilino, D.B. Ground and Excited States of Bis-4-Methoxybenzyl-Substituted Diketopyrrolopyrroles: Spectroscopic and Electrochemical Studies. *ChemPlusChem* **2019**, *84*, 1413–1422. [[CrossRef](#)] [[PubMed](#)]
61. Ponsot, F.; Desbois, N.; Bucher, L.; Berthelot, M.; Mondal, P.; Gros, C.P.; Romieu, A. Near-infrared emissive bacteriochlorin-diketopyrrolopyrrole triads: Synthesis and photophysical properties. *Dye. Pigment.* **2019**, *160*, 747–756. [[CrossRef](#)]
62. Langhals, H.; Potrawa, T.; Noth, H.; Linti, G. Der Einfluß von Packungseffekten auf die Feststofffluoreszenz von Diketopyrrolopyrrolen. *Angew. Chem.* **1989**, *101*, 497–499. [[CrossRef](#)]
63. Langhals, H.; Demmig, S.; Potrawa, T. The Relation between Packing Effects and Solid State Fluorescence of Dyes. *J. Prakt. Chem.* **1991**, *333*, 733–748. [[CrossRef](#)]
64. Lorenz, I.-P.; Limmert, M.; Mayer, P.; Piotrowski, H.; Langhals, H.; Poppe, M.; Polborn, K. DPP Dyes as Ligands in Transition-Metal Complexes. *Chem. A Eur. J.* **2002**, *8*, 4047–4055. [[CrossRef](#)]
65. Kirkus, M.; Knippenberg, S.; Beljonne, D.; Cornil, J.; Janssen, R.A.J.; Meskers, S.C.J. Synthesis and Optical Properties of Pyrrolo[3,2-b]pyrrole-2,5(1H,4H)-dione (iDPP)-Based Molecules. *J. Phys. Chem. A* **2013**, *117*, 2782–2789. [[CrossRef](#)] [[PubMed](#)]
66. Liu, J.; Walker, B.; Tamayo, A.; Zhang, Y.; Nguyen, T.-Q. Effects of Heteroatom Substitutions on the Crystal Structure, Film Formation, and Optoelectronic Properties of Diketopyrrolopyrrole-Based Materials. *Adv. Funct. Mater.* **2012**, *23*, 47–56. [[CrossRef](#)]

67. Fischer, G.M.; Ehlers, A.P.; Zumbusch, A.; Daltrozzi, E. Near-Infrared Dyes and Fluorophores Based on Diketopyrrolopyrroles. *Angew. Chem. Int. Ed.* **2007**, *46*, 3750–3753. [[CrossRef](#)]
68. Fischer, G.M.; Isomäki-Krondahl, M.; Göttker-Schnetmann, I.; Daltrozzi, E.; Zumbusch, A. Pyrrolopyrrole Cyanine Dyes: A New Class of Near-Infrared Dyes and Fluorophores. *Chem. A Eur. J.* **2009**, *15*, 4857–4864. [[CrossRef](#)] [[PubMed](#)]
69. Shimizu, S.; Iino, T.; Araki, Y.; Kobayashi, N. Pyrrolopyrrole aza-BODIPY analogues: A facile synthesis and intense fluorescence. *Chem. Commun.* **2013**, *49*, 1621. [[CrossRef](#)]
70. Marks, T.; Daltrozzi, E.; Zumbusch, A. Azacyanines of the Pyrrolopyrrole Series. *Chem. A Eur. J.* **2014**, *20*, 6494–6504. [[CrossRef](#)]
71. Yue, W.; Suraru, S.-L.; Bialas, D.; Müller, M.; Würthner, F. Synthesis and Properties of a New Class of Fully Conjugated Azahexacene Analogues. *Angew. Chem.* **2014**, *126*, 6273–6276. [[CrossRef](#)]
72. Yu, J.; Li, N.; Chen, D.-F.; Luo, S.-W. Catalytic enantioselective C(sp³)-H functionalization: Intramolecular benzylic[1,5]-hydride shift. *Tetrahedron Lett.* **2014**, *55*, 2859–2864. [[CrossRef](#)]
73. Luňák, S., Jr.; Vyňuchal, J.; Vala, M.; Havel, L.; Hrdina, R. The synthesis, absorption and fluorescence of polar diketo-pyrrolopyrroles. *Dyes Pigm.* **2009**, *82*, 102–108. [[CrossRef](#)]
74. Vala, M.; Krajčovič, J.; Luňák, S., Jr.; Ouzzane, I.; Bouillon, J.-P.; Weiter, M. HOMO and LUMO energy levels of N, N'-dinitrophenyl-substituted polar diketopyrrolopyrroles (DPPs). *Dyes Pigm.* **2014**, *106*, 136–142. [[CrossRef](#)]
75. Vala, M.; Weiter, M.; Vyňuchal, J.; Toman, P.; Lunák, S. Comparative Studies of Diphenyl-Diketo-Pyrrolopyrrole Derivatives for Electroluminescence Applications. *J. Fluoresc.* **2008**, *18*, 1181–1186. [[CrossRef](#)] [[PubMed](#)]
76. Luňák, S., Jr.; Vala, M.; Vyňuchal, J.; Ouzzane, I.; Horáková, P.; Možíšková, P.; Eliáš, Z.; Weiter, M. Absorption and fluorescence of soluble polar diketo-pyrrolo-pyrroles. *Dye. Pigm.* **2011**, *91*, 269–278. [[CrossRef](#)]
77. Kanbara, T.; Yamagata, T.; Kuwabara, J. Synthesis and Photophysical Properties of Diketopyrrolopyrrole-Based Near-Infrared Dyes. *Heterocycles* **2014**, *89*, 1173. [[CrossRef](#)]
78. Zhang, L.; Zou, L.-Y.; Guo, J.-F.; Ren, A.-M. Theoretical investigation on the one- and two-photon responsive behavior of fluoro-ride ion probes based on diketopyrrolopyrrole and its π -expanded derivatives. *New J. Chem.* **2016**, *40*, 4899–4910. [[CrossRef](#)]
79. Bürckstümmer, H.; Weissenstein, A.; Bialas, D.; Würthner, F. Synthesis and Characterization of Optical and Redox Properties of Bithiophene-Functionalized Diketopyrrolopyrrole Chromophores. *J. Org. Chem.* **2011**, *76*, 2426–2432. [[CrossRef](#)]
80. Zhang, K.; Wucher, P.; Marszalek, T.; Babics, M.; Ringk, A.; Blom, P.W.M.; Beaujuge, P.M.; Pisula, W. Long-Range Molecular Self-Assembly from π -Extended Pyrene-Functionalized Diketopyrrolopyrroles. *Chem. Mater.* **2018**, *30*, 5032–5040. [[CrossRef](#)]
81. Patil, Y.; Misra, R. Rational molecular design towards NIR absorption: Efficient diketopyrrolopyrrole derivatives for organic solar cells and photothermal therapy. *J. Mater. Chem. C* **2019**, *7*, 13020–13031. [[CrossRef](#)]
82. Dhar, J.; Venkatramiah, N.; Patil, S. Photophysical, electrochemical and solid state properties of diketopyrrolopyrrole based molecular materials: Importance of the donor group. *J. Mater. Chem. C* **2014**, *2*, 3457–3466. [[CrossRef](#)]
83. Canivet, J.; Yamaguchi, J.; Ban, I.; Itami, K. Nickel-Catalyzed Biaryl Coupling of Heteroarenes and Aryl Halides/Triflates. *Org. Lett.* **2009**, *11*, 1733–1736. [[CrossRef](#)]
84. Ackermann, L.; Vicente, R.; Kapdi, A.R. Transition-Metal-Catalyzed Direct Arylation of (Hetero)Arenes by C-H Bond Cleavage. *Angew. Chem. Int. Ed.* **2009**, *49*, 9792–9826. [[CrossRef](#)] [[PubMed](#)]
85. Cardoza, S.; Shrivash, M.K.; Das, P.; Tandon, V. Strategic Advances in Sequential C-Arylations of Heteroarenes. *J. Org. Chem.* **2021**, *86*, 1330–1356. [[CrossRef](#)]
86. Zhang, J.; Kang, D.-Y.; Barlow, S.; Marder, S.R. Transition metal-catalyzed C-H activation as a route to structurally diverse di(arylthiophenyl)-diketopyrrolopyrroles. *J. Mater. Chem.* **2012**, *22*, 21392–21394. [[CrossRef](#)]
87. Wakioka, M.; Takahashi, R.; Ichihara, N.; Ozawa, F. Mixed-Ligand Approach to Palladium-Catalyzed Direct Arylation Polymerization: Highly Selective Synthesis of π -Conjugated Polymers with Diketopyrrolopyrrole Units. *Macromolecules* **2017**, *50*, 927–934. [[CrossRef](#)]
88. Ni, Z.; Wang, H.; Dong, H.; Dang, Y.; Zhao, Q.; Zhang, X.; Hu, W. Mesopolymer synthesis by ligand-modulated direct arylation polycondensation towards n-type and ambipolar conjugated systems. *Nat. Chem.* **2019**, *11*, 271–277. [[CrossRef](#)]
89. Hagui, W.; Doucet, H.; Soulé, J.-F. Application of Palladium-Catalyzed C(sp²)-H Bond Arylation to the Synthesis of Polycyclic (Hetero)Aromatics. *Chem* **2019**, *5*, 2006–2078. [[CrossRef](#)]
90. Roger, J.; Požgan, F.; Doucet, H. Ligand-Free Palladium-Catalyzed Direct Arylation of Thiazoles at Low Catalyst Loadings. *J. Org. Chem.* **2009**, *74*, 1179–1186. [[CrossRef](#)]
91. Purc, A.; Espinoza, E.M.; Nazir, R.; Romero, J.J.; Skonieczny, K.; Jeżewski, A.; Larsen, J.M.; Gryko, D.T.; Vullev, V.I. Gating That Suppresses Charge Recombination—The Role of Mono-N-Arylated Diketopyrrolopyrrole. *J. Am. Chem. Soc.* **2016**, *138*, 12826–12832. [[CrossRef](#)] [[PubMed](#)]
92. Krzeszewski, M.; Espinoza, E.M.; Červinka, C.; Derr, J.B.; Clark, J.A.; Borchardt, D.; Beran, G.J.O.; Gryko, D.T.; Vullev, V.I. Dipole Effects on Charge Transfer are Enormous. *Angew. Chem. Int. Ed.* **2018**, *57*, 12365–12369. [[CrossRef](#)]
93. Ryu, H.G.; Mayther, M.F.; Tamayo, J.; Azarias, C.; Espinoza, E.M.; Banasiewicz, M.; Łukasiewicz, Ł.G.; Poronik, Y.M.; Jeżewski, A.; Clark, J.; et al. Bidirectional Solvatochromism of a Pyrrolo[3,2-b]pyrrole–Diketopyrrolopyrrole Hybrid. *J. Phys. Chem. C* **2017**, *122*, 13424–13434. [[CrossRef](#)]
94. McCusker, C.E.; Hablot, D.; Ziessel, R.; Castellano, F.N. Triplet State Formation in Homo- and Heterometallic Diketopyrrolopyrrole Chromophores. *Inorg. Chem.* **2014**, *53*, 12564–12571. [[CrossRef](#)] [[PubMed](#)]

95. McCusker, C.E.; Hablot, D.; Ziessel, R.; Castellano, F.N. Metal Coordination Induced π -Extension and Triplet State Production in Diketopyrrolopyrrole Chromophores. *Inorg. Chem.* **2012**, *51*, 7957–7959. [[CrossRef](#)] [[PubMed](#)]
96. Tamayo, A.B.; Tantiwivat, M.; Walker, B.; Nguyen, T.-Q. Design, Synthesis, and Self-assembly of Oligothiophene Derivatives with a Diketopyrrolopyrrole Core. *J. Phys. Chem. C* **2008**, *112*, 15543–15552. [[CrossRef](#)]
97. Frisch, M.J.; Trucks, G.W.; Schlegel, H.B.; Scuseria, G.E.; Robb, M.A.; Cheeseman, J.R.; Scalmani, G.; Barone, V.; Petersson, G.A.; Nakatsuji, H.; et al. *Gaussian 16, Revision A.03*; Gaussian, Inc.: Wallingford, CT, USA, 2016.
98. Zhao, Y.; Truhlar, D.G. The M06 suite of density functionals for main group thermochemistry, thermochemical kinetics, non-covalent interactions, excited states, and transition elements: Two new functionals and systematic testing of four M06-class functionals and 12 other functionals. *Theor. Chem. Acc.* **2008**, *120*, 215–241. [[CrossRef](#)]